Environmental Research 285 (2025) 122549

Contents lists available at ScienceDirect

Environmental Research

journal homepage: www.elsevier.com/locate/envres

Simulated aging processes induced significant changes in redox properties of biochar for chromate reduction

Beiping Zhang [a], Shaofeng Zhou [b,*], Xianhuai Huang [a], Yuchao Tang [a], Kun Wang [a], Yong Yuan [c,**]

[a] Key Laboratory of Water Pollution Control and Wastewater Reuse of Anhui Province, Anhui Provincial Key Laboratory of Environmental Pollution Control and Resource Reuse, Anhui Jianzhu University, Hefei, China
[b] Guangdong Provincial Key Laboratory of Microbial Culture Collection and Application, State Key Laboratory of Applied Microbiology Southern China, Institute of Microbiology, Guangdong Academy of Sciences, Guangzhou, 510070, China
[c] Guangzhou Key Laboratory Environmental Catalysis and Pollution Control, Guangdong Key Laboratory of Environmental Catalysis and Health Risk Control, School of Environmental Science and Engineering, Institute of Environmental Health and Pollution Control, Guangdong University of Technology, Guangzhou, 510006, China

ARTICLE INFO

Keywords:
Aged biochar
Redox activities
Electron transfer capacity
PLS modeling
Cr(VI) reduction

ABSTRACT

Biochar, a carbon-rich material, features a well-developed porous structure and abundant oxygen-containing functional groups that collectively facilitate efficient electron transfer. Upon environmental exposure, biochar generally undergoes aging processes like temperature fluctuations, water erosion, and natural oxidation, leading to significant changes in its physical and chemical properties. However, research addressing the impact of aging processes on biochar's redox behavior remain limited. In this study, we systematically investigated the effects of three simulated aging processes (i.e., chemical oxidation, acidification, and freeze–thaw cycling) on the redox properties of wheat straw-derived biochar. Electrochemical analysis suggested that the oxidized biochar (OBC) presented higher redox-active performance and partial least squares modeling revealed that enhancements in electron transfer capacity (ETC) were closely linked to the enrichment of phenolic hydroxyl and quinone groups, increases in specific surface area, and the development of conjugated π–π* structures. Specifically, the electron donating capacity and electron accepting capacity of (OBC) increased from 0.051 to 0.066 mmol e^-/g_c and from 0.083 to 0.151 mmol e^-/g_c, respectively. Functionally, biochar facilitated the reduction of Cr(VI) as an electron donor and it could mediate electron transfer as an electron shuttler when lactate was introduced. The combined system of biochar and lactate achieved Cr(VI) reduction rates approximately two to three times greater than those attained by either biochar or lactate alone. This synergistic enhancement was positively correlated with the ETC of biochar. This work provides critical insights into the aging-induced evolution of biochar's redox properties, highlighting its sustained and enhanced potential as a sustainable electron shuttle for long-term remediation of redox-sensitive environmental contaminants.

1. Introduction

Chromium (Cr) is a heavy metal frequently encountered in natural environments (Liu et al., 2019). This element, especially in its hexavalent form (Cr(VI)), raises significant concerns due to its emissions and leakages from industrial activities and anthropogenic actions (Dhal et al., 2013). This Cr(VI) contamination negatively impacts aquatic ecosystems, threatening the survival and reproductivity of aquatic organisms (McClain et al., 2017). Moreover, chromium pollution exhibits a propensity for bioaccumulation along the food chain, thereby posing severe health risks to humans (Dhal et al., 2013; Richard and Bourg, 1991). The U.S. Environmental Protection Agency specifies that the total Cr concentration in drinking water should not exceed 100 μg L^{-1} (Coyte et al., 2020). The reduction of Cr(VI) to Cr(III) is an effective strategy for remediating Cr(VI)-contaminated environment, as Cr(III) is less toxic and it can be stabilized by readily precipitating as $Cr(OH)_3$ (Crean et al., 2012; Deng et al., 2021). Various methods, including electrochemical processes, photocatalytic, bioremediation, and chemical reduction with redox-active agents (e.g., biochar, zero-valent iron, and sulfides), have been currently used to remove Cr(VI) (Du et al., 2019; He et al., 2024;

* Corresponding author.
** Corresponding author.
E-mail addresses: zsfking@hotmail.com (S. Zhou), yyuan2017@gdut.edu.cn (Y. Yuan).

https://doi.org/10.1016/j.envres.2025.122549
Received 19 June 2025; Received in revised form 5 August 2025; Accepted 6 August 2025
Available online 8 August 2025
0013-9351/© 2025 Elsevier Inc. All rights are reserved, including those for text and data mining, AI training, and similar technologies.

Liu et al., 2019; Yang et al., 2024; Zhang et al., 2023).

Biochar, a collection of carbon-rich materials derived from pyrolysis of diverse biomass under oxygen-limited conditions, has received intensive attention due to its versatile promising applications for tackling environmental issues such as carbon sequestration, soil remediation, and contaminant adsorption (Lu et al., 2022; Yang et al., 2024). The pyrolysis process can yield biochar with a condensed aromatic carbon structure and an abundance of redox-active functional groups, including hydroxyl, quinone, and amino groups (Yuan et al., 2017; Zhang et al., 2019b). It has been extensively reported that Cr(VI) could be reduced to less toxic Cr(III) by biochar through phenolic−OH and quinone-type moiety (Yuan et al., 2017). In addition to be electron donor, recent studies have indicated that biochar could also act as a "shuttle" or "mediator" in biogeochemical and pollutant redox reactions. For example, peanut shell biochar could mediate the reduction of Cr(VI) by small molecular weight organic acids (Xu et al., 2019). Therefore, biochar can effectively reduce highly toxic Cr(VI) and stabilize the resulting Cr(III) through adsorption and precipitation (Shang et al., 2021; Zhu et al., 2020). Additionally, organic acids are prevalent in the environment and participate in various redox-active reactions, biochar can accept electrons from small organic acids to complete the reduction of Cr(VI) (Xu et al., 2019). As a result, biochar exhibits considerable potential as a sustainable and effective Cr(VI) remediation. However, upon introduction into aquatic or terrestrial environments, biochar undergoes a range of physicochemical transformations, collectively termed "aging" driven by microbial activity, temperature fluctuations, and dynamic redox conditions (Xu et al., 2019; Lu et al., 2022). Previous studies have demonstrated that chemical aging enhanced the abundance of redox-active groups (e.g., hydroxyl, quinone, and carboxyl groups) and improved the microporous structure of biochar (Chen et al., 2022; Mia et al., 2017a). Extensive evidence indicated that the electron transfer capacity (ETC) of biochar was strongly correlated with surface properties, encompassing both chemical structures (e.g., oxygen-containing functional groups) and physical architectures (e.g., specific surface area and conjugated domains). Notably, quinone and phenolic moieties serve as redox-active mediators that facilitate electron exchange, while an expanded specific surface area provides enhanced redox-active interfaces (Yuan et al., 2017). Based on these findings, it could be reasonably inferred that the aging process likely influences the redox activity of biochar and its capacity to adsorb and reduce Cr(VI). In this regard, a mechanistic understanding of how aging affects the redox dynamics of biochar is therefore essential for accurately evaluating its long-term efficacy in environmental pollutant remediation. Nonetheless, comprehensive studies addressing this relationship remain limited.

In this study, wheat straw-derived biochar was subjected to acidification, oxidation, and freeze-thaw cycles that mimicked natural aging processes of which the effects on biochar's electrochemical properties were systematically evaluated. The ETC of the biochar before and after aging processes were investigated via a series of electrochemical methods including cyclic voltammetry (CV) and chronoamperometry. Concurrently, the structural properties were quantified by BET specific surface area (S_{BET}), the surface functionalities including redox-active moieties were evaluated by the qualitative characterization of X-ray photoelectron spectroscopy (XPS) and Fourier transform infrared (FTIR) spectroscopy. To further investigate the environmental impact of these redox properties, Cr(VI) was selected as the model pollutant to examine the capability of aged biochar functioning as both an electron donor and an electron mediator for the reduction of Cr(VI). The adsorption and reduction effects of aged biochar on Cr(VI) were systematically analyzed using a Partial Least Squares (PLS) model, which revealed key correlations between ETC performance and physicochemical characteristics of the biochars.

2. Materials and methods

2.1. Chemicals

The waste wheat straw for biochar preparation was collected from Yangjiang, JiangSu Province, China. Chemicals used in this study were purchased from Macklin Inc. (Shanghai, China) and Aladdin Chemical Reagent Co. Ltd (Shanghai, China). A complete list of chemicals is provided in Supporting Information (SI) Text S1.

2.2. Biochar preparation and aging processes

The wheat straw was air-dried at room temperature and then further ground to pass through a 100-mesh sieve. Afterwards, the biomass powders were pyrolyzed in a tube furnace under an oxygen-limited conditions with a continuous flow of nitrogen gas at 500 °C for 2 h, following a heating rate of 5 °C min^{-1}. The obtained powders were washed three times by deionized water, dried at 45 °C overnight, and collected as pristine biochar (BC) samples.

The aged biochar was prepared following three different aging processes (i.e., acidification, oxidation, and freeze-thaw cycles). In the acidification process, 0.5 g pristine biochar and 40 mL acid solution (20 % HNO_3 and 60 % H_2SO_4 at a volume ration of 1:3) were mixed and continuously stirred at 70 °C for 6 h. The acidified biochar (ABC) was repeatedly rinsed with ionized water until a neutral pH was achieved. For oxidation of biochar, 0.5 g pristine biochar was mixed with 40 mL H_2O_2 (5 %, v/v) at 80 °C and continuously stirred for 12 h. Then the biochar was rinsed repeatedly with deionized water until the pH value of the filtrate stabilized. The resulted oxidized biochar (OBC) was dried at 45 °C for 48 h prior to use. In the freeze-thaw process, 0.5 g pristine biochar was suspended in deionized water at a biochar-to-water ratio (w/v) of 1:25. The suspension was heated to 80 °C for 8 h, followed by freezing at −20 °C for another 12 h. This freeze-thaw cycle was repeated four times. Subsequently, the obtained biochar (FBC) was rinsed with deionized water to neutral pH and dried in an oven. All biochar samples were dried at 45 °C for 48 h in a drying oven and subsequently ground to pass through a 200-mesh sieve.

2.3. Biochar characterization

The surface morphologies and elemental abundances of the pristine and aged biochar samples were examined XPS. The FTIR analysis provides the bonding information of the organic molecules, which was implemented using an infrared spectrometer (Tensor 37, Bruker Corp., Germany) operated in transmission mode. The zeta potential was measured using a Malvern Zetasizer (Zetasizer NANO ZS, Malvern, UK). More characterization techniques and detailed information are described in SI Texts S2.

2.4. Electrochemical analysis

The qualification of biochar ETC was determined by the combination of electron donating capacity (EDC) and electron accepting capacity (EAC) (Kluepfel et al., 2014). In detail, a three-electrode system with a glassy carbon cylinder (10 mL) was employed as the working electrode, while a platinum plate (1 × 1 cm^2) and an Ag/AgCl electrode (0.197 V vs. standard hydrogen electrode) served as the counter electrode (CE) and reference electrode (RE), respectively. Note that all potentials presented in this work were read against this Ag/AgCl electrode. The reactor was filled with 5 mL of phosphate buffer (0.1 M) solution (PBS, pH = 7) containing 0.1 M KCl as the electrolyte. The mediated electrochemical reduction (MER) and oxidation (MEO) were anaerobically conducted under a poised potential of −0.49V and +0.61V, respectively (Kluepfel et al., 2014). The diquat dibromide (DQ) monohydrate and 2, 2′-azino-bis (3-ethylbenzothiazoline-6-sulfonic acid (ABTS) were chosen as the external mediators for MER and MEO reactions, respectively. The

system current was continuously recorded when gradient increasing amounts of biochar (0.1 mg–0.5 mg) were spiked into the cylinder after the system current stabilized. The values of EDC and EAC were calculated following eqs (1) and (2) (Kluepfel et al., 2014).

$$EDC = \frac{\int \frac{I_{red}}{F} dt}{m} \quad (1)$$

$$EAC = \frac{\int \frac{I_{ox}}{F} dt}{m} \quad (2)$$

Where the I_{red} and I_{ox} were the reductive and oxidative currents, respectively. *F* is the Faraday constant (96485 [C/mol$_{e^-}$]), and m (g biochar) is the dosage amount of biochar added in the system. The values were calculated in duplicate.

The details of CV tests are described in SI Texts S3. All electrochemical experiments were carried out at room temperature using an electrochemical workstation (CHI 660D, Chenhua, China).

2.5. Cr(VI) reduction by biochar

A Cr(VI) stock solution with an initial concentration of 50 mg Cr(VI) L^{-1} was prepared by dissolving $K_2Cr_2O_7$ in a 0.1M KCl solution. The Cr (VI) reduction experiments were conducted in a 50 mL centrifuge tube containing 20 mg biochar and 20 mL stock solution, unless otherwise stated. The stock solution contained 10 mM sodium lactate as the electron donor. Experiments without biochar or sodium lactate were set as control groups. The pH value of the mixture was adjusted to pH = 4.0 using 1 mM HCl and 1 mM KOH solutions. The solution was incubated at 25 °C, 125 rpm for 70 h. Samples were taken out at regular time intervals and filtered using a 0.45-μm filter. The concentrations of Cr(VI) were measured using a UV–vis spectrometer at a wavelength of 540 nm (Zhu et al., 2020). The total Cr concentrations were measured using a flame atomic absorption spectrometer (AAS) and the Cr(III) concentrations were calculated by abstracting the Cr(VI) concentration from the total Cr concentration. The differences between the final and initial total Cr concentrations in solution were recognized as the amounts of Cr(VI) adsorbed by biochar. All experiments were conducted at least duplicate.

2.6. PLS modeling and data analysis

The Partial least squares **(**PLS**)** modeling is utilized to determine the relationship between the redox properties (EDC and EAC) of biochar and the ratio of functional groups and structural indexes. Cross-validation was used to find the optimum component index for PLS (Tuppurainen et al., 2000). To assess modeling, the diagnostic criteria such as quantitative measurement parameters were used to for explain variation (R^2) and anticipated variation (Q^2), as well as the outlier index (DCrit) (Tugizimana et al., 2016). SIMCA 14 software (Umetrics AB, Umeå, Sweden) was used for PLS modeling.

3. Results and discussion

3.1. Physicochemical properties of the aged biochar

The aging processes significantly induced changes of surface chemistry. The alterations in surface functional groups of biochar after different aging processes were analyzed using FT-IR spectroscopy, as illustrated in Fig. 1. Notably, the -OH stretching vibrations around 3400 cm^{-1} were significantly stronger in ABC and OBC compared to BC and FBC, indicating the enrichment of hydroxyl groups during acidification and oxidation treatments (Chen et al., 2008). The bands corresponding to phenolic-OH stretching (1400 - 1450 cm^{-1}) were substantially stronger in OBC than those in BC, while ABC exhibited a reverse trend with reduced intensity (Chen et al., 2012). Previous research established a correlation between the phenolic hydroxyl groups and the

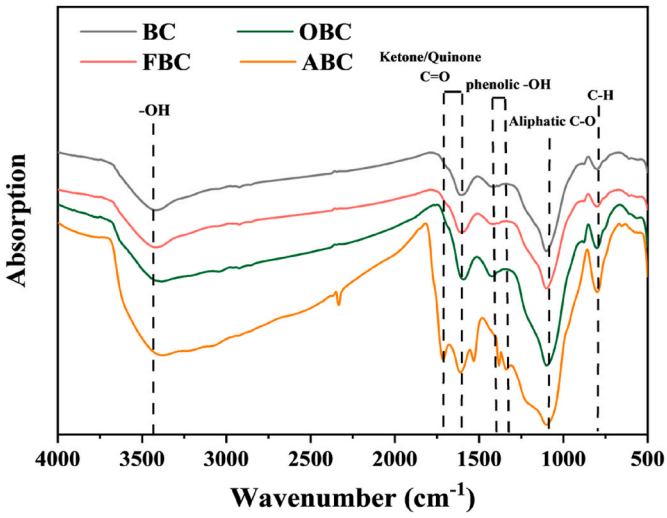

Fig. 1. Fourier transform infrared spectra of all biochar samples.

electrochemical properties of biochar, emphasizing their potential importance in electron transfer dynamics (Kluepfel et al., 2014). In addition, the C=O stretching vibrations at 1670 cm^{-1} were notably intensified in ABC, and quinone-related C=O stretching bands (1610 cm^{-1}) displayed higher absorption intensities in both ABC and OBC compared to BC and FBC (Qian and Chen, 2014; Zhu et al., 2020). Compared with BC, there were both stronger C-O and C-H stretching vibrations at respective 1100 and 800 cm^{-1} in ABC and OBC (Chen et al., 2008; Qian and Chen, 2014). These findings suggested that the acidification and oxidation aging processes significantly increased the abundance of oxygen-containing functional groups on the surface of biochar, which might be advantageous for electron transfer and adsorption capacity of biochar.

Particularly, the formation of hydrophilic and polar functional groups was changed by altering the elemental compositions and surface constructions of biochar, as evidenced by the changes in C, N, and O concentrations in XPS analysis, as well as the specific surface area (SSA) and pore structure from Brunauer-Emmett-Teller test (Table S1). Compared with untreated biochar, both ABC and OBC exhibited a similar increase in oxygen contents, whereas the carbon contents decreased significantly. Among all the biochar samples, the OBC experienced the most pronounced elemental changes, with increases in O, N, O/C, and (O + N)/C by 37.84 %, 32.72 %, 33.33 %, and 36.84 %, respectively. These changes suggested that oxidative aging promoted the incorporation of oxygen- and nitrogen-containing functional groups, potentially enhancing the biochar's hydrophilicity and polarity (Mia et al., 2017a). In contrast, the nitrogen content in FBC decreased that was likely due to the removal of volatile compounds and N-containing fractions during the freeze-thaw aging process. The SSA of FBC decreased from 25.59 (BC) to 17.84 $m^2\ g^{-1}$ after freeze-thaw aging process, while the SSA of ABC and OBC increased to 26.12 $m^2\ g^{-1}$ and 30.03 $m^2\ g^{-1}$, respectively. However, the micropore area (MPA) and micropore volume (MPV) of all biochar samples decreased after aging processes, indicating that aging processes inevitably compromised the pore structure to some extent. These findings were consistent with previous studies that suggested oxidation process would lower the SSA of biochar, partly due to the blocking of pores in the oxidized biochar with biochar-derived dissolved organic matter (Mia et al., 2017b).

The C 1s and O 1s peak spectra of the original and aged biochar are shown in Fig. S1 (a)–(h). The C 1s spectrum of biochar is deconvoluted into five distinct peaks corresponding to sp^2, sp^3, hydroxyl groups (C-OH), carbonyl or carboxyl groups (i.e., C=O, COOR, and COOH), and π-π* conversion, respectively (Okpalugo et al., 2005). Similarly, the O 1s spectrum is resolved into four peaks attributed to quinone groups,

carbonyl groups (C=O), ether/hydroxyl groups (C-O/C-OH), and carboxylic acid groups (Zhang et al., 2025). The relative proportions of these functional groups, calculated based on the C 1s and O 1s peak spectra, are presented in Fig. 2(a) and (b). The surface of the original biochar was predominantly composed of carbon in the form of sp^2 and sp^3 bonds. However, all aging processes significantly reduced the proportion of sp^2 carbon, especially the acidification and oxidation exerted the most pronounced effects on the structure of sp^2 carbon. This suggested that the aging process disrupted the aromatic structure of biochar, likely through oxidative degradation of the sp^2 hybridized carbon network. Notably, the fitting results of both C 1s and O 1s spectra indicated a decrease in carboxyl group content in FBC, while the carboxyl (-COOH) and hydroxyl (C-OH) group contents increased in ABC and OBC. This observation is consistent with the FTIR spectra results, further confirming that acidification and oxidation introduced additional oxygen-containing functional groups onto the biochar surface. These findings demonstrated that chemically aged biochar resulted in higher oxygen content compared to unaged biochar. Additionally, the content of redox-active quinone groups decreased after freeze-thaw aging, whereas acidification and oxidation increased the quinone group content. Since quinone groups are primarily responsible for biochar's EAC (Kluepfel et al., 2014), these changes suggested that freeze-thaw aging might reduce the redox activity of biochar which is discussed in the following section. Furthermore, all aging processes accelerated the π-π* transitions in biochar, indicating changes in the conjugated carbon structure. The XPS analysis results collectively indicated that freeze-thaw aging had a minimal impact on surface functional groups, while acidification and oxidation aging promoted the conversion of C-C/C=C bonds to oxidized states, leading to an increase in oxygen-containing functional groups on the biochar surface.

The surface electrical properties of biochar were reflected by Zeta potential. As shown in Fig. S2, the Zeta potentials of biochar significantly varied with pH. At pH = 2, the Zeta potentials of BC, FBC, ABC and OBC were 10.15, 3.32, −13.77, and −6.92 mV, respectively. The observed changes in Zeta potential were consistent with the introduction of oxygen-containing functional groups during acidification and oxidation aging, which increased the negative surface charge density. This implied that the Cr(VI), primarily in anion forms in aqueous solution, could integrate with biochar due to the electrostatic repulsion (Yang et al., 2022). In contrast, freeze-thaw aging had a less pronounced effect on the Zeta potential, further supporting the notion that aging via variation of temperatures had a limited impact on surface functional groups. These findings highlighted that different aging processes distinctly altered the surface chemistry and electrical properties of biochar. Acidification and oxidation aging significantly increased the oxygen content and negative surface charge, enhancing the biochar's capacity for cation adsorption. In contrast, freeze-thaw aging primarily affected the physical structure and redox-active groups, with minimal impact on surface functionalization. These insights were critical for understanding the environmental behavior and applications of aged biochar in pollutant adsorption and redox-related processes.

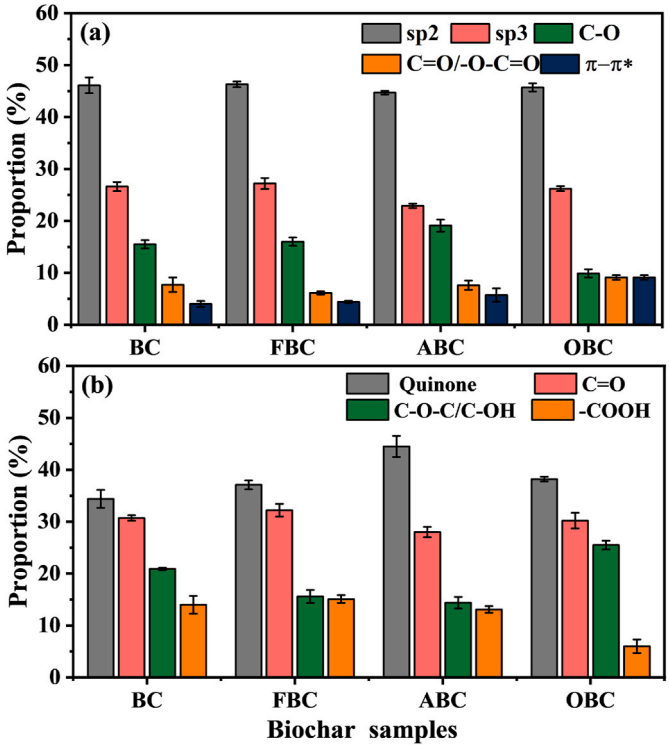

Fig. 2. Dominant functional groups of (a) C-bond class and (b) O-bond class calculated from XPS spectra of biochar samples.

3.2. Mediated electrochemical properties of the aged biochar

The mediated electrochemical properties of biochar were connected with the values of ETC. As shown in Fig. 3 and S3, the EDC and EAC values of pristine biochar were 0.051 mmol e^-/g_c and 0.083 mmol e^-/g_c, respectively. After aging, the EDC values of FBC and ABC slightly decreased to 0.042 and 0.045 mmol e^-/g_c, respectively, while the EDC value of OBC significantly increased to 0.066 mmol e^-/g_c. On the other hand, the EAC value of FBC slightly decreased to 0.081 mmol e^-/g_c, whereas the EAC values of ABC and OBC increased by 65 % and 81 %, respectively, reaching 0.137 and 0.151 mmol e^-/g_c, respectively. These results demonstrated that oxidation aging process enhanced both EAC and EDC, attributed to the formation of oxygen-containing quinoid structures. Conversely, acidification aging process manifested a trade-off effect with EDC reduction coinciding with EAC augmentation. Notably, the disruption of the aromatic carbon network during freeze-thaw aging process might reduce both EDC and EAC of FBC. Generally, the oxidation aging process realized higher abundant of redox moieties in OBC which enabled the higher total electron transfer capacity (ETC = EAC + EDC) to the OBC compared with other aging processes.

A mediated electrochemical method involved (dimethylaminomethy) Ferrocene (FcDMAM) and hexa-ammineruthenium(III) chloride (Ru^{3+}) as redox probes were conducted for visualizing redox properties of biochar samples (Kim et al., 2014; Yuan et al., 2018). Biochar generally mediated redox reactions of FcDMAM and Ru^{3+} in a wide range of potential (E_h) (Kim et al., 2017). Fig. 4a and **b** show small

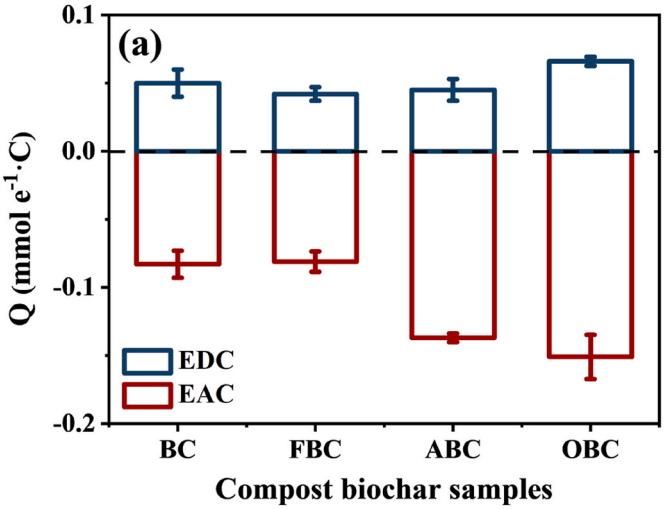

Fig. 3. EDC and EAC values of modified biochar.

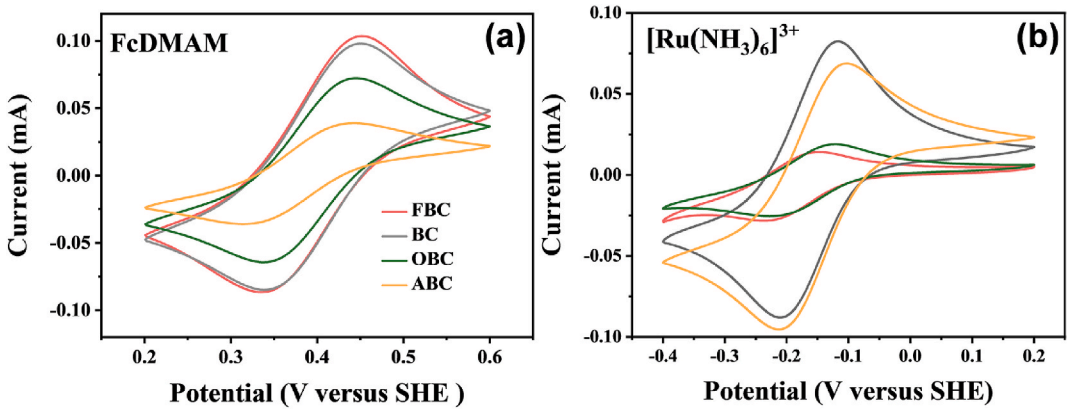

Fig. 4. Cyclic voltammetry (CV) curves of all biochars in (a) FcDMAM solution and (b) $[Ru(CN)_6]^{3+}$ solution at a scan rate of 100 mV s^{-1}.

FcDMAM and Ru^{3+} oxidation and reduction currents at 0.34 V and −0.21 V, respectively, when the potential cycled between 0.6 Vand −0.4 V at a scan rate of 100 mV s^{-1}. Compared to the BC, the OBC and ABC shown weaker FcDMAM oxidation peaks, probably due to their reduced Zeta potential causing electrostatic repulsion toward the negatively charged FcDMAM and imposing kinetic barriers to interfacial electron transport processes. Notably, OBC exhibited an enhancement in Ru^{3+} reduction current compared to pristine BC, whereas ABC and FBC displayed suppression of Ru^{3+} reduction efficiency. This divergence aligned mechanistically with values of EDC, suggesting that surface charge modulation governed redox pathway selectivity in aged biochar. Notably, the OBC presented superior redox performance with the highest amplification current among the four BCs. These findings are consistent with previous studies that evidenced chemical aging process could alter the structural properties of biochar by introducing some oxygen-containing functional groups as redox-active sites (Cai et al., 2025).

3.3. Correlation between the biochar redox activity and the surface structure

Assessing the electron transfer capacity of biochar solely on the characterization of functional groups may be insufficient. Previous studies have demonstrated that the electron transfer capacity of biochar was not exclusively dependent on quinones and phenolic groups (Li et al., 2020). Therefore, the PLS model was employed to explore the relationships between the redox activity, structure characteristics, and surface properties of biochar.

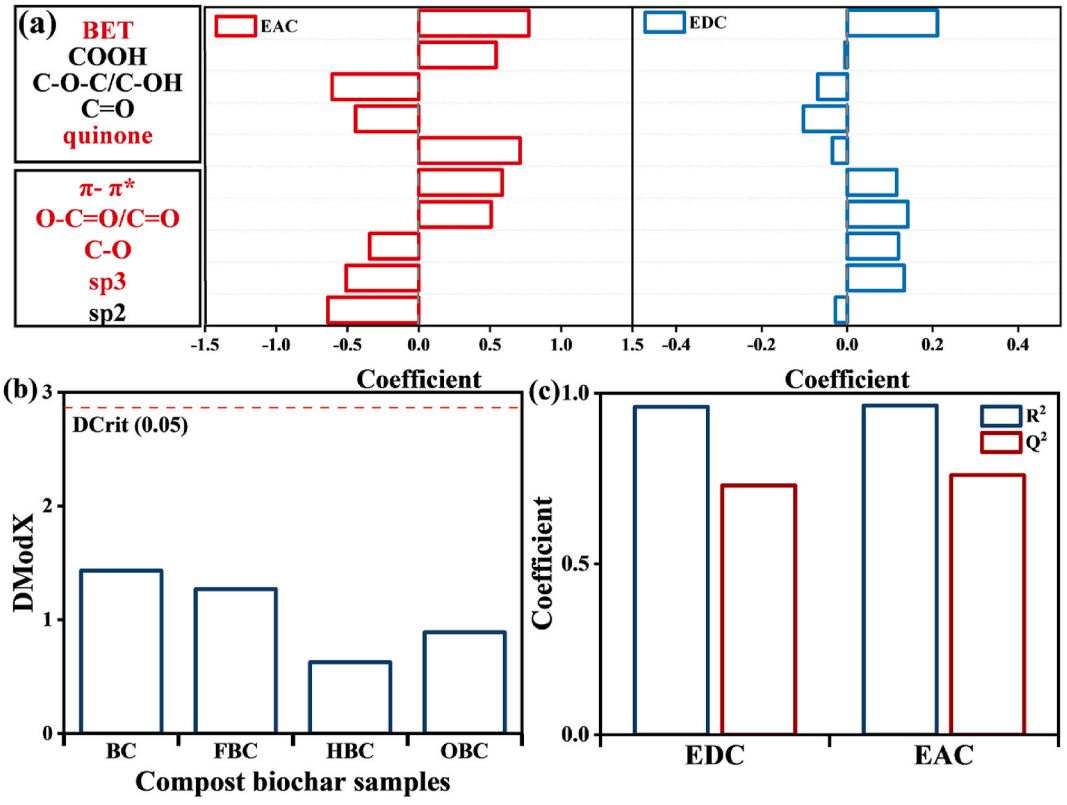

Fig. 5. PLS model diagram (a) Correlation coefficient of independent variables, with red emphasizing VIP coefficients greater than or equal to 1; (b) DModX plot, where the dashed line represents the critical distance with a 95 % tolerance interval (DCrit0.05); (c) Cumulative explained variance parameter R^2 value and cumulative predicted variance parameter Q^2 value. (For interpretation of the references to colour in this figure legend, the reader is referred to the Web version of this article.)

In the PLS model, the EDC and EAC were designated as dependent variables, while the specific surface area (S_{BET}) and contents of functional groups were set as independent variables. The relative proportions of functional groups on the biochar surface were determined by fitting the C 1s and O 1s spectra obtained from XPS. The regression coefficients corresponding to independent variables influencing EDC and EAC are displayed in Fig. 5a. Particular attention was given to variables with a variable importance in projection (VIP) score ≥1, which indicated a significant contribution to the predictive power of the model (Wei et al., 2015). The DModX plot (Fig. 5b) indicated no discernible outliers at a significant threshold of 0.05, confirming the robustness of the PLS model. As shown in Fig. 5c, the values of cumulated explained variation parameters (R^2) for the EDC and EAC were 0.97 and 0.96, respectively, whereas the values of cumulated predicted variation parameter (Q^2) were 0.81 and 0.79, respectively. The results presented in Fig. 5a indicate that the most significant independent variables (VIP ≥1) are SSA, quinone groups, sp^3 carbon phase, π-π* structure, and O-containing groups (C–O and O–C=O or C=O bondings). The SSA had a positive correlation with both EDC and EAC, likely attributed to the increased exposure of redox-active sites. Quinone groups showed a positive correlation with EAC, consistent with their well-established role as potent redox mediators. Previous studies demonstrated that the EAC of biochar was largely governed by the abundance and types of quinone groups (Kluepfel et al., 2014). Similarly, the sp^3 hybridized carbon content associated with aliphatic structures, and C–O groups which were prone to oxidation, showed a positive correlation to EDC. The π-π* structure, primarily derived from poly-condensed aromatic carbons, was positively correlated with both EDC and EAC values. Furthermore, the observed relationship between lactone groups and electron storage capacity aligned with results aforementioned, reinforcing their relevance in biochar redox functionality (Li et al., 2020).

Previous studies had established that the electron transfer capacity of biochar was predominantly governed by oxygen-containing functional groups (Kluepfel et al., 2014). Through systematic investigation, this study elucidated distinct quantitative structure-activity relationships between the intrinsic structural characteristics (including specific surface area and π-π*) and its electrochemical properties of biochar. The SSA had a positive correlation with both EDC and EAC, likely attributed to the increased exposure of redox-active sites. It was possibly because of the aging processes would induce significant changes in surficial structure (e.g., collapse of internal pore spaces), as the SSA and FTIR-related analysis indicated. This would accordingly result in more microporous structures as potential active sites to promote electron transfer capabilities of biochar, indicating that the pore structure had an indirect relationship with the electron transfer ability of biochar. Furthermore, the π-π*, functioning as electron delocalization pathways, exhibited synergistic enhancing effects on both EDC and EAC, substantiating the pivotal regulatory role of the carbon matrix configuration in charge transport dynamics.

3.4. Cr(VI) removal by different aged biochar

The initial pH significantly affected the removal efficiencies of Cr (VI), as it influenced both the adsorption efficiency of biochar and the reducing rate of Cr(VI). As shown in Fig. S4, the aged biochar exhibited maximum Cr(VI) removal efficiency (46 %–76 %) at an initial pH 2.0. The removal efficiency decreased as the pH increased, which was primarily attributed to the lower reducibility of biochar at higher pH. Under acidic conditions, biochar contained a substantial number of oxygen-containing functional groups (e.g., -COOH) as electron donors to convert Cr(VI) into less toxic Cr(III) through a reduction reaction, given that the Cr(VI) mainly exists in the form of $HCrO_4^-$ in this environment due to protonation. The lower negative charge density and smaller molecular size of Cr(VI) made it more easily being adsorbed by biochar through electrostatic attraction and coordination (Zhang et al., 2019a). This interaction facilitated the adsorption and subsequent reduction of Cr(VI) on the biochar surface.

The effects of lactate on Cr(VI) reduction was presented in Fig. S5. It shows that the lactate could slightly reduce Cr(VI) without biochar, resulting in observed accumulation of Cr(III). That evidences lactate could be the electron donor for Cr(VI) reduction. However, this effect was incomparable with that of group in which aged biochar was added, which was consistent with previous studies (Xu et al., 2019). Nevertheless, the increase of Cr(III) accumulation in the presence of aged biochar indicated the electron flow to Cr(VI) was enhanced.

The Cr(VI) removal rates, utilizing biochar as the electron donor for reduction, were presented in Fig. 6a. The OBC significantly enhanced the Cr(VI) removal efficiency to 76 %, while 66 % Cr(VI) were removed in BC-group. In contrast, the ABC and FBC decreased the Cr(VI) removal efficiencies to 61 % and 57 %, respectively. As shown in Fig. 6b, the reduction efficiency of Cr(VI) (referred as the generation of Cr(III)) was 18 % in BC-group, while those in the presence of FBC, ABC, and OBC were 16 %, 22 %, and 25 %, respectively. The reduction process followed first order kinetics, suggested that the reaction rate was proportional to the concentration of Cr(VI). Previous characterizations of biochar's ETC indicated that the EDC correlated with Cr(III) generation, confirming that biochar could act as an electron donor, directly supplying electrons for the reduction of Cr(VI).

To further investigate the potential of biochar as electron shuttles, lactate was introduced as an electron donor for the reduction of Cr(VI). The results are shown in Fig. 6 c and d. The coexistence of lactate and biochar efficiently facilitated Cr(VI) reduction to Cr(III). The Cr(VI) removal efficiencies of BC, OBC, and ABC were strengthened to 57 %, 93 % and 71 %, respectively, while it reduced to only 33 % in the FBC-group. Among the removed Cr(VI), 25 %, 18 %, 33 %, and 43 % of the total Cr(VI) were removed via reduction in the groups of BC, FBC, ABC, and OBC, respectively. These results suggested that biochar could serve as an electron shuttle as well to mediate electron transfer from lactate to Cr(VI). The enhanced performance in OBC-group might be attributed to its higher electron transfer capacity and additional redox-active functional groups introduced during oxidation aging process.

As illustrated in Fig. S6 a and b, the removal of Cr(VI) by all biochar primarily proceeded via adsorption. However, the introduction of lactate led to divergent responses among the biochar. The removal efficiency of FBC remained unchanged, whereas BC exhibited a notable decline in Cr(VI) removal, accompanied by a substantial decrease in adsorbed Cr(VI). This phenomenon might be attributed to lactate competitively occupying the active adsorption sites on BC, thereby limiting its adsorption capacity. In contrast, both OBC and ABC demonstrated remarkably enhanced Cr(VI) removal efficiency in the presence of lactate, with reduction process becoming the dominant removal pathway. These findings suggested that the aging processes of oxidation and acidification promoted the formation of stable electron transfer pathways in OBC and ABC, enabling them to function effectively as electron shuttles and facilitate electron transfer from lactate to Cr(VI). While FBC retained partial Cr(VI) removal capacity via adsorption, its reductive capabilities were significantly impaired due to the loss of active sites during aging process.

Based on the aforementioned results, it is reasonable to conclude that the enhanced reduction of Cr(VI) could be attributed to electron transfer capacities of biochar. The correlations between Cr(III) accumulation and the EDC/EAC of biochar during Cr(VI) reduction are shown in Fig. S7 a and b. The strong correlation between EDC and Cr(III) accumulation in lactate-free systems suggested that biochar primarily functioned as an electron donor to directly reduce Cr(VI). On the other hand, when lactate was introduced as an exogenous electron source, the ETC exhibited a strong correlation with Cr(III) accumulation (R^2 = 0.95, Fig. S7 b). This shift indicated a mechanistic transition in which the role of biochar transitioned from a direct electron donor to an electron shuttle, mediating electron transfer from lactate to Cr(VI) in the presence of organic substrates. These findings highlight biochar's dual role in Cr(VI) reduction, demonstrating its versatility in redox processes and

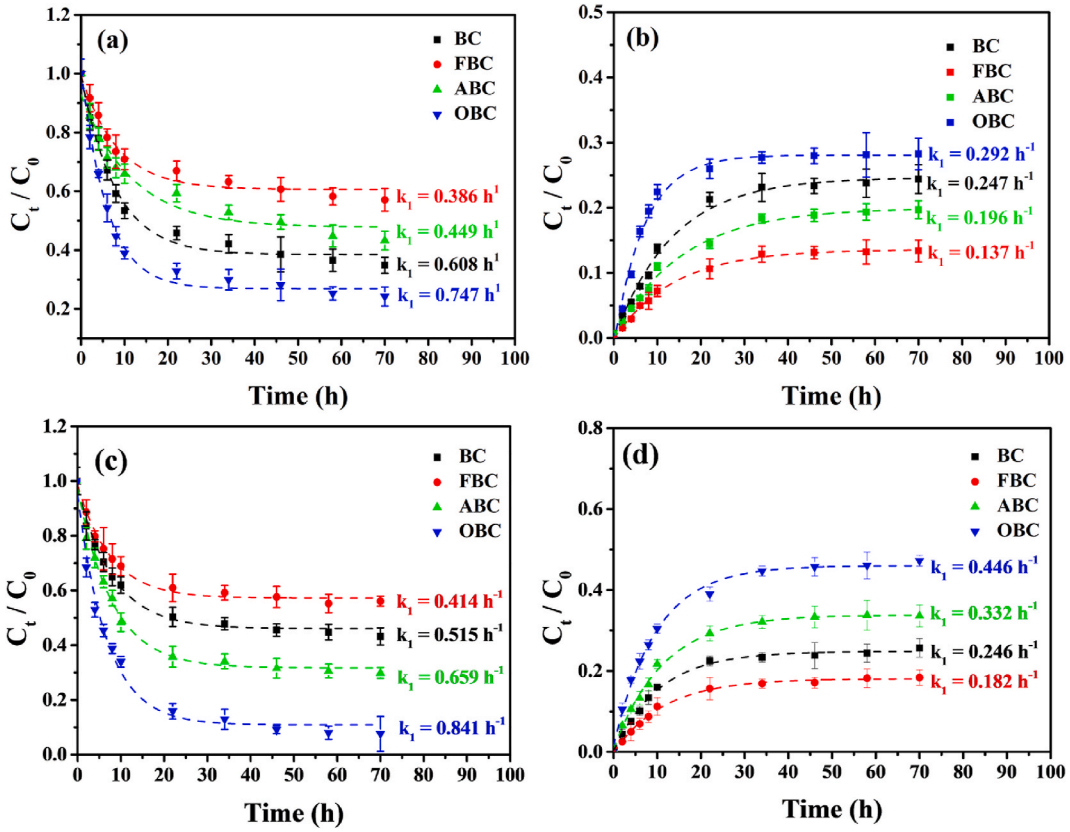

Fig. 6. (a) Cr(VI) removal and (b) Cr(III) produced profiles of all biochar; (c) Cr(VI) removal and (d) Cr(III) produced in presence of lactate.

potential for contaminant remediation.

3.5. Environmental implication

Biochar is increasingly used in environmental remediation due to its redox activity and surface reactivity. However, biochar's redox behaviors and their pollutant remediation capacities are strongly influenced by environmental aging processes, such as oxidative weathering, and seasonal freeze–thaw cycles commonly occurring in natural soils and sediments. These conditions potentially promote chemical transformations that influence surface functionality, π–π* conjugation, and electron transfer capacity (ETC) of biochar. In this study, we demonstrated that aged biochars after different aging processes showed differentiated performance in Cr(VI) reduction as electron donors or shuttles. For a long-term perspective, strategies for optimizing biochar performance for targeted remediation should be in accordance of biochar's specific application environment. For example, pre-oxidation treatments for tailoring surface modifications can be implemented to enhance redox-active functional groups or adjusting the application environment (e.g., co-adding organic electron donors) can amplify electron shuttling effects. These findings suggest that a better understanding and manipulation of biochar's aging trajectory can improve the precision and efficiency of redox-sensitive contaminant control in diverse environmental settings.

4. Conclusions

The objective of this study aimed to investigate the effects of various aging processes on the redox activity of biochar. The freeze-thaw cycle significantly disrupted the microporous structure of the biochar surface, leading to a reduction in its specific surface area. In contrast, both oxidation and acidification aging enriched the abundance of oxygen-containing functional groups on the biochar surface, including carboxyl, carbonyl, quinones, and phenolic groups. This increase in functional groups subsequently elevated the polarity of biochar and facilitates π-π* interactions. Changes in surface structure and functional groups directly influenced the redox activity of biochar, thereby improving its electron transfer capacity. Consequently, the Cr(VI) reduction efficiency of aged biochar (i.e., OBC) was nearly doubled. The PLS model analysis revealed that the redox activity of biochar was closely associated with the surface redox-active functional groups and the increase in specific surface area, along with enhanced π-π* interactions, further augmented the electron transfer capacity of oxidized biochar.

CRediT authorship contribution statement

Beiping Zhang: Writing – original draft, Visualization, Validation, Methodology, Formal analysis. **Shaofeng Zhou:** Writing – review & editing, Supervision, Funding acquisition. **Xianhuai Huang:** Supervision, Funding acquisition. **Yuchao Tang:** Formal analysis. **Kun Wang:** Formal analysis. **Yong Yuan:** Supervision, Funding acquisition, Conceptualization.

Declaration of competing interest

The authors declare that they have no known competing financial interests or personal relationships that could have appeared to influence the work reported in this paper.

Acknowledgments

This work was financially supported by the program for the National Key Research and Development Program of China (2023YFC3205705), Young Talent Project of GDAS (2024GDASQNRC-0201), GDAS' Special Project of Science and Technology Development (2024GDASZH-

2024010102), and the Science and Technology Project of Guangzhou (2024A04J3593)

Appendix A. Supplementary data

Supplementary data to this article can be found online at https://doi.org/10.1016/j.envres.2025.122549.

Data availability

Data will be made available on request.

References

Cai, H.X., Liu, Y.Q., Zhang, Z.P., Wang, X.C., Song, X.M., Wen, Y.J., 2025. Enhanced removal of endocrine disrupting chemicals by chemically modified biochar: efficiency and mechanisms. J. Ind. Eng. Chem. 144, 192–209. https://doi.org/10.1016/j.jiec.2024.10.012.

Chen, B.L., Zhou, D.D., Zhu, L.Z., 2008. Transitional adsorption and partition of nonpolar and polar aromatic contaminants by biochars of pine needles with different pyrolytic temperatures. Environ. Sci. Technol. 42, 5137–5143. https://doi.org/10.1021/es8002684.

Chen, X., Gao, X.D., Yu, P.F., Spanu, L., Hinojosa, J., Zhang, S.Q., Long, M.C., Alvarez, P. J.J., Masiello, C.A., 2022. Rapid simulation of decade-scale charcoal aging in soil: changes in physicochemical properties and their environmentalimplications. Environ. Sci. Technol. 57 (1), 128–138. https://doi.org/10.1021/acs.est.2c04751, 2022.

Chen, Z.M., Chen, B.L., Chiou, C.T., 2012. Fast and slow rates of naphthalene sorption to biochars produced at different temperatures. Environ. Sci. Technol. 46, 11104–11111. https://doi.org/10.1021/es302345e.

Coyte, R.M., McKinley, K.L., Jiang, S., Karr, J., Dwyer, G.S., Keyworth, A.J., Davis, C.C., Kondash, A.J., Vengosh, A., 2020. Occurrence and distribution of hexavalent chromium in groundwater from North Carolina, USA. Sci. Total Environ. 711, 135135. https://doi.org/10.1016/j.scitotenv.2019.135135.

Crean, D.E., Coker, V.S., van der Laan, G., Lloyd, J.R., 2012. Engineering biogenic magnetite for sustained Cr(VI) remediation in flow-through systems. Environ. Sci. Technol. 46, 3352–3359. https://doi.org/10.1021/es2037146.

Deng, N., Li, Z.X., Zuo, X.B., Chen, J.W., Shakiba, S., Louie, S.M., Rixey, W.G., Hu, Y.D., 2021. Coprecipitation of Fe/Cr hydroxides with organics: roles of organic properties in composition and stability of the coprecipitates. Environ. Sci. Technol. 55, 4638–4647. https://doi.org/10.1021/acs.est.0c04712.

Dhal, B., Thatoi, H.N., Das, N.N., Pandey, B.D., 2013. Chemical and microbial remediation of hexavalent chromium from contaminated soil and mining/metallurgical solid waste: a review. J. Hazard. Mater. 250, 272–291. https://doi.org/10.1016/j.jhazmat.2013.01.048.

Du, X.D., Yi, X.H., Wang, P., Zheng, W.W., Deng, J.G., Wang, C.C., 2019. Robust photocatalytic reduction of Cr(VI) on UiO-66-$NH_{2(Zr/Hf)}$ metal-organic framework membrane under sunlight irradiation. Chem. Eng. J. 356, 393–399. https://doi.org/10.1016/j.cej.2018.09.084.

He, K., Lai, Y.F., Wang, S.C., Gong, L., He, F., 2024. Mechanochemical synthesis of manganese-modified microscale zerovalent iron for efficient Cr(VI) removal: performance and mechanism. ACS ES&T Engg 4, 2553–2562. https://doi.org/10.1021/acsestengg.4c00316.

Kim, E., Kang, M., Tschirhart, T., Malo, M., Dadachova, E., Cao, G., Yin, J.J., Bentley, W. E., Wang, Z., Payne, G.F., 2017. Spectroelectrochemical reverse engineering demonstrates that melanin's redox and radical scavenging activities are linked. Biomacro 18, 4084–4098. https://doi.org/10.1021/acs.biomac.7b01166.

Kim, E., Liu, Y., Leverage, W.T., Yin, J.J., White, I.M., Bentley, W.E., Payne, G.F., 2014. Context-dependent redox properties of natural phenolic materials. Biomacro 15, 1653–1662. https://doi.org/10.1021/bm500026x.

Kluepfel, L., Keiluweit, M., Kleber, M., Sander, M., 2014. Redox properties of plant biomass-derived black carbon (biochar). Environ. Sci. Technol. 48, 5601–5611. https://doi.org/10.1021/es500906d.

Li, S.S., Shao, L.M., Zhang, H., He, P.J., Lü, F., 2020. Quantifying the contributions of surface area and redox-active moieties to electron exchange capacities of biochar. J. Hazard. Mater. 394. https://doi.org/10.1016/j.jhazmat.2020.122541.

Liu, X.L., Dong, H.L., Zeng, Q., Yang, X.W., Zhang, D.L., 2019. Synergistic effects of reduced nontronite and organic ligands on Cr(VI) reduction. Environ. Sci. Technol. 53, 13732–13741. https://doi.org/10.1021/acs.est.9b04769.

Lu, Y., Cai, Y., Zhang, S., Zhuang, L., Hu, B., Wang, S., Chen, J., Wang, X., 2022. Application of biochar-based photocatalysts for adsorption-(photo) degradation/reduction of environmental contaminants:mechanism,challenges and perspective. Biochar 4, 45. https://doi.org/10.1007/s42773-022-00173-y, 2022.

McClain, C.N., Fendorf, S., Webb, S.M., Maher, K., 2017. Quantifying Cr(VI) production and export from serpentine soil of the California coast range. Environ. Sci. Technol. 51, 141–149. https://doi.org/10.1021/acs.est.6b03484.

Mia, S., Dijkstra, F.A., Singh, B., 2017a. Aging induced changes in biochar's functionality and adsorption behavior for phosphate and ammonium. Environ. Sci. Technol. 51, 8359–8367. https://doi.org/10.1021/acs.est.7b00647.

Mia, S., Dijkstra, F.A., Singh, B., 2017b. Aging induced changes in biochar's functionality and adsorption behavior for phosphate and ammonium. Environ. Sci. Technol. 51, 8359–8367. https://doi.org/10.1021/acs.est.7b00647.

Okpalugo, T.I.T., Papakonstantinou, P., Murphy, H., McLaughlin, J., Brown, N.M.D., 2005. High resolution XPS characterization of chemical functionalised MWCNTs and SWCNTs. Carbon 43, 153–161. https://doi.org/10.1016/j.carbon.2004.08.033.

Qian, L.B., Chen, B.L., 2014. Interactions of aluminum with biochars and oxidized biochars: implications for the biochar aging process. J. Agric. Food Chem. 62, 373–380. https://doi.org/10.1021/jf404624h.

Richard, F.C., Bourg, A.C.M., 1991. Aqueous geochemistry of chromium-a review. Water Res. 25, 807–816. https://doi.org/10.1016/0043-1354(91)90160-r.

Shang, H., Zhang, S.C., Zhu, X.D., 2021. Biomass cellulose component and Fe mineral catalysis help Cr(VI) to realize almost 100% pyrolysis reduction efficiency. ACS ES&T Engg 1, 1441–1448. https://doi.org/10.1021/acsestengg.1c00174.

Tugizimana, F., Steenkamp, P.A., Piater, L.A., Dubery, I.A., 2016. A conversation on data mining strategies in LC-MS untargeted metabolomics: pre-processing and pre-treatment steps. Metabolites 6. https://doi.org/10.3390/metabo6040040.

Tuppurainen, K.A., Ruokojärvi, P.H., Asikainen, A.H., Aatamila, M., Ruuskanen, J., 2000. Chlorophenols, as precursors of PCDD/Fs in incineration processes: correlations, PLS modeling, and reaction mechanisms. Environ. Sci. Technol. 34, 4958–4962. https://doi.org/10.1021/es991429x.

Wei, M.G., Geladi, P., Lestander, T.A., Xie, G.H., Xiong, S.J., 2015. Multivariate modelling on biomass properties of cassava stems based on an experimental design. Anal. Bioanal. Chem. 407, 5443–5452. https://doi.org/10.1007/s00216-015-8706-2.

Xu, Z.B., Xu, X.Y., Tao, X.Y., Yao, C.B., Tsang, D.C.W., Cao, X.D., 2019. Interaction with low molecular weight organic acids affects the electron shuttling of biochar for Cr (VI) reduction. J. Hazard. Mater. 378. https://doi.org/10.1016/j.jhazmat.2019.05.098.

Yang, D.X., Liu, T., Deng, R.Y., Xian, Z.H., Chen, Y., 2024. Porous biochar-driven innovative Cr(VI) reduction and resource recovery. Chem. Eng. J. 499. https://doi.org/10.1016/j.cej.2024.156556.

Yang, F., Jiang, Y.T., Dai, M., Hou, X.T., Peng, C.S., 2022. Active biochar-supported iron oxides for Cr(VI) removal from groundwater: kinetics, stability and the key role of FeO in electron-transfer mechanism. J. Hazard. Mater. 424. https://doi.org/10.1016/j.jhazmat.2021.127542.

Yuan, Y., Bolan, N., Prévoteau, A., Vithanage, M., Biswas, J.K., Ok, Y.S., Wang, H.L., 2017. Applications of biochar in redox-mediated reactions. Bioresour. Technol. 246, 271–281. https://doi.org/10.1016/j.biortech.2017.06.154.

Yuan, Y., Cai, X.X., Tan, B., Zhou, S.G., Xing, B.S., 2018. Molecular insights into reversible redox sites in solid-phase humic substances as examined by electrochemical in situ FTIR and two-dimensional correlation spectroscopy. Chem. Geol. 494, 136–143. https://doi.org/10.1016/j.chemgeo.2018.07.029.

Zhang, B.P., Zhou, S.F., Zhou, L.H., Wen, J.L., Yuan, Y., 2019a. Pyrolysis temperature-dependent electron transfer capacities of dissolved organic matters derived from wheat straw biochar. Sci. Total Environ. 696. https://doi.org/10.1016/j.scitotenv.2019.133895.

Zhang, M.F., Yang, M., Yaguchi, M., Jintoku, H., Sakurai, S., Futaba, D., 2025. Understanding and controlling the oxidation degree of single-wall carbon nanotubes: a comparative study of treatment processes. Carbon 237. https://doi.org/10.1016/j.carbon.2025.120132.

Zhang, X., Meng, G., Hu, J., Xiao, W., Li, T., Zhang, L., Chen, P., 2023. Electroreduction of hexavalent chromium using a porous titanium flow-through electrode and intelligent prediction based on a back propagation neural network. Front. Environ. Sci. Eng. 17, 97. https://doi.org/10.1007/s11783-023-1697-x.

Zhang, Y., Xu, X.Y., Zhang, P.Y., Zhao, L., Qiu, H., Cao, X.D., 2019b. Pyrolysis-temperature depended quinone and carbonyl groups as the electron accepting sites in barley grass derived biochar. Chemosphere 232, 273–280. https://doi.org/10.1016/j.chemosphere.2019.05.225.

Zhu, S.S., Huang, X.C., Yang, X.B., Peng, P., Li, Z.P., Jin, C., 2020. Enhanced transformation of Cr(VI) by heterocyclic-n within nitrogen-doped biochar: impact of surface modulatory persistent free radicals (PFRs). Environ. Sci. Technol. 54, 8123–8132. https://doi.org/10.1021/acs.est.0c02713.